FULL PAPER

Anatomy

Morphological analysis of cell distribution and network structure via gap junctions in swine corneal stroma

Nobutaka HOSHINO[1], Kazushige TAKEHANA[1], Marina HOSOTANI[1], Kiyokazu KAMETANI[1], Tomohito IWASAKI[2], Yasuhiro HASEGAWA[2], Hiromi UEDA[1], Takafumi WATANABE[1]*

[1]Department of Veterinary Anatomy, School of Veterinary Medicine, Rakuno Gakuen University, Hokkaido, Japan

[2]Department of Food Science and Human Wellness, College of Agriculture, Food and Environment Science, Rakuno Gakuen University, Hokkaido, Japan

ABSTRACT. Because of corneal transplantation limitations, there is a need for cornea-specific regenerative medicine. The development of such regenerative medicine has been delayed because of the complex and unique structure of the corneal stroma. Few studies have explored the corneal stroma cell distribution and cell types *in vivo*. This study investigated regional differences in morphological characteristics and distributions of corneal keratocytes and immunocompetent cells in the corneal stroma to clarify their functions and structural characteristics. The porcine eyeballs were subjected to light microscopy, transmission electron microscopy, scanning electron microscopy, and immunofluorescence staining analyses. Corneal cells were primarily located in the limbus, rather than the center of the cornea; the long keratocyte diameter was largest on the epithelial side of the corneal limbus, while the short diameter was largest on the endothelial side of the central cornea. Moreover, there were significantly more corneal cells on the epithelial side than on the endothelial side in both the central and limbus areas. Gap junctions between cells in the corneal stroma were present on the surfaces of cytoplasmic processes. Many cytoplasmic processes were scattered throughout the corneal stroma; they were connected both vertically and horizontally, forming an intercellular network. Additionally, immunocompetent cells on the epithelial side suggested to participate in this network via gap junctions. The morphology of keratocytes and immunocompetent cells on the epithelial side suggests that they play important roles in corneal homeostasis.

KEYWORDS: corneal keratocytes, corneal stroma, electron microscopy, gap junction, swine

The cornea is located in the anterior 20% of the eye; this structure is non-vascular and is nourished by aqueous humor [2]. Additionally, the epithelial layer is a unique tissue that does not undergo keratinization or pigmentation; it remains transparent. The cornea is divided into five layers: anterior corneal epithelium (corneal epithelium), anterior border plate (Bowman's membrane), corneal stroma, posterior border plate (Descemet's membrane), and posterior corneal epithelium (corneal endothelium). The corneal stroma consists of collagen fibers and corneal keratocytes [2]. The cornea is mostly collagen (i.e., 70% of its dry weight) [22]. Collagen fibrils in the corneal stroma are regularly arranged and form a thin laminar structure of approximately 1 μm thickness; fibrils travel in the same direction in an orderly manner [36]. They cross each other at a specific angle and are arranged parallel to the corneal surface, forming a corneal stromal layer of approximately 300 layers [36]. Collagen fibril diameter ranges from 20 to 30 nm; this uniform thickness and regular arrangement are essential for corneal transparency [36]. In addition to keratocytes, myeloid-derived migratory cells (e.g., lymphocytes, macrophages, and some granulocytes) are reportedly present in the corneal stroma [2, 25, 40]. The presence of antigen-presenting cells, such as Langerhans cells and dendritic cells, has recently been reported in the corneal epithelium, as well as the corneal stroma; it is presumably involved in rejection during transplantation [10, 11, 26, 40].

The overall corneal thickness differs between the central and limbal areas; the limbal area is thicker than the central area in humans, dogs, and cattle [24]. The overall thickness of the cornea is determined by collagen fibrils and proteoglycans [1, 9, 30, 33]. These

collagen-producing keratocytes reside between collagen layers; they extend cytoplasmic processes connected by gap junctions [28, 38]. Because corneal thickness varies according to collagen fibril and proteoglycan content, regional differences are expected in terms of corneal keratocytes involved in collagen production.

Corneal transplantation is indicated in corneal diseases with irreversible opacity [7]. However, corneal transplantation is associated with donor shortages and rejection problems. Thus, there is a need for cornea-specific regenerative medicine. Currently, cell sheets of corneal epithelium and corneal endothelium have been developed; epithelial sheets have been used in human medicine, while endothelial sheets have been experimentally transplanted into animals [27, 35]. Additionally, cell sheets using induced pluripotent stem cells are currently used in clinical treatment [12, 29]. However, the development of regenerative medicine for the corneal stroma, which constitutes the majority of the cornea, has been delayed because of the complex and unique structure of this light-transmitting layer; it has also been delayed because of immune-mediated rejection [2, 34].

Studies of culture techniques and cell sheets associated with corneal transplantation [25] have been conducted with respect to the corneal stroma, but there have been few studies regarding the cell distribution and cell types *in vivo*. Therefore, this study aims to analyze the morphological characteristics and distribution of corneal keratinocytes and immunocompetent cells in the corneal stroma to clarify their functional and structural features using porcine eyes, which are relatively easy to obtain for clinical application to companion animals.

MATERIALS AND METHODS

Experimental animals

Thirty porcine (three-way crossbreed of Landrace, Great Yorkshire, and Duroc; approximately 6 months old) eyeballs were obtained from a slaughterhouse for use in this study. The pigs used in this study were sacrificed in a commercial slaughterhouse that complies with the slaughterhouse Laws of Japan and operates under guidelines for industrial animal welfare licensed by the Japanese government.

Observation of cells in corneal stroma

Light microscopy analysis of stromal cell distribution: Corneal sclera fragments were prepared from 10 porcine eyes that had been pre-fixed in 3.0% glutaraldehyde and 0.1 M phosphate buffer (pH 7.4). The samples were then post-fixed in 1.0% osmium tetroxide solution, dehydrated in an ethanol series according to the usual method, and embedded in Quetol 812 (Nisshin EM, Tokyo, Japan). Sections (1.5 µm thickness) were prepared on an ultramicrotome (Reichert Supernova; Leica, Wetzler, Germany), stained with toluidine blue, and observed using a light microscope at 40× magnification. The number of corneal keratocytes per field of view (0.054 mm^2) was measured using ImageJ software, version 1.44; mean ± standard deviation values were recorded.

Transmission electron microscopy analysis of corneal keratocytes: Using three eyes of the above-mentioned embedded samples, ultrathin sections (80 nm thickness) were generated with an ultramicrotome. After double staining with 1% uranium acetate for 5 min and 2% lead citrate for 30 sec, the samples were observed using a transmission electron microscope (JEM-1220; JEOL, Tokyo, Japan) at an accelerating voltage of 80 kV.

Scanning electron microscopy analysis of corneal keratocytes: Samples that included epithelium and endothelium were obtained from 10 eyes; each endothelium was held with ophthalmic tweezers, peeled by rubbing with an ophthalmic surgical absorbent sponge, and immersed overnight in 0.1 M phosphate buffer solution (pH 7.4) and 3% acetic acid to swell the corneal stroma. The swollen corneal stroma was divided into epithelial and endothelial sides with a razor and pre-fixed in 3% glutaraldehyde and 0.1 M phosphate buffer (pH 7.4) for >3 hr. After connective tissue had been removed using the hydrochloric acid-collagenase method, the cells were post-fixed in 1.0% osmium tetroxide for 1 hr. In accordance with the usual method, the samples were dehydrated in an ethanol series, subjected to exchange with t-butyl alcohol, and lyophilized in a freeze-drying apparatus (JFD-300; JEOL). The freeze-dried samples were then adhered to the sample table and an osmium coating was applied using an osmium plasma coater (NL-OPC; Japan Laser Electronics Co., Ltd., Nagoya, Japan). Observations were performed using a scanning electron microscope (JSM-5200; JEOL) at an acceleration voltage of 5 or 10 kV.

Observation of gap junctions among keratocytes

Immunofluorescence staining analysis of connexin 43: Corneal samples were dissected from nasal side to ear side with a razor blade, then fixed in 4% paraformaldehyde in 0.1 M phosphate buffer (pH 7.4) at 4°C overnight; subsequently, they were washed several times in phosphate buffer and embedded in paraffin wax in accordance with standard procedures. Paraffin sections (2 µm thickness) were cut and mounted on MAS-coat glass slides (Matsunami Glass Ind., Ltd., Osaka, Japan). Deparaffinized sections were immersed in antigen retrieval solution (Histo VT One; Nacalai Tesque Inc., Kyoto, Japan) and heated at 70°C for 20 min, then incubated with blocking reagent (Blocking One Histo; Nacalai Tesque Inc.) for 10 min at room temperature. After the sections had been washed with phosphate-buffered saline (PBS), they were incubated for 24 hr at 4°C in a humid chamber with primary antibody, rabbit anti-connexin 43/GJA1 (NB110-55546; Novus Biologicals LLC., Centennial, CO, USA) diluted 1:100 with immunoreactivity sensitizing reagent (Can Get Signal; TOYOBO, Osaka, Japan). Sections were then washed three times with PBS and incubated for 3 hr in a dark chamber with CF 488-conjugated goat anti-rabbit IgG serum (diluted 1:300; Biotium, Hayward, CA, USA). Sections were washed again with PBS, then coverslipped with aqueous mounting medium containing 4′,6-diamidino-2-phenylindole (DAPI) (Fluoro-KEEPER; Nacalai Tesque Inc.); finally, they were observed on a fluorescence microscope (ECLIPSE Ni-U; Nikon, Tokyo, Japan).

Transmission electron microscopy analysis of cell junctions: Corneal samples were cut into 2 mm × 1 mm × 1 mm blocks, then immediately fixed by immersion in a half-Karnovsky solution (2% paraformaldehyde + 2.5% glutaraldehyde in 0.1 M cacodylate buffer,

pH 7.4) at 4°C overnight. Tissue membrane structural contrast was enhanced for electron microscopy via heavy metal block staining, as previously described [36]. Briefly, the fixed samples were washed four times with 0.1 M cacodylate buffer (4 min each); immersed in 2% OsO$_4$ (TAAB Laboratories Equipment Ltd., Berks, UK) and 1.5% potassium ferrocyanide trihydrate (Nacalai Tesque Inc.) in 0.1 M cacodylate buffer (pH 7.4) for 1 hr at 4°C; washed four times with distilled water (4 min each); immersed in 0.1% thiocarbohydrazide (Sigma Aldrich, Tokyo, Japan) for 20 min at room temperature; washed four times with distilled water (4 min each); immersed in 2% OsO$_4$ for 30 min at room temperature; washed four times with distilled water (4 min each); immersed in 1% uranyl acetate at 4°C overnight; washed four times with distilled water (4 min each); and immersed in Walton's lead aspartate solution at 60°C for 30 min. Subsequently, the tissues were dehydrated in an ethanol series, transferred to QY-1, and embedded in epoxy resin (Quetol 812; Nisshin EM). After polymerization, the tissue blocks were sliced into 100-nm-thick sections from epithelium to endothelium using an ultramicrotome (EM UC7; Leica). The sections were collected on a single-hole grid with Holmbar support membrane and observed using an electron microscope (HT-7700; Hitachi High Technology, Tokyo, Japan) at an acceleration voltage of 80 kV.

Observations of immunocytes in corneal stroma

Analysis of ATPase-positive immunocompetent cells: Immunocytes in the corneal stroma were observed by histochemistry using adenosine triphosphatase (ATP) ase-specific detection of antigen-presenting cells, such as Langerhans cells and dendritic cells [33]. Eyes were fixed in 4% paraformaldehyde at 4°C for 12 to 24 hr. They were then immersed in 5% sucrose/0.1 M PBS for 4 hr at 4°C; this was followed by immersion in 10% sucrose/0.1 M PBS for 4 hr at 4°C, then in 20% sucrose/0.1 M PBS for 1 hr at 4°C. The eyes were embedded using optimal cutting temperature (OCT) compound and frozen in dry ice plus ethanol. Frozen thin sections (20 μm thickness) were prepared using a freezing microtome (CM-1500; Leica). The sections were washed three times with 0.15 M NaCl for 10 min at 4°C, then reacted with Pb solution containing ATP as the substrate for 15 min at 37°C. Control sections were reacted with ATP-free Pb solution as a control for 15 min at 37°C. The sections were then washed three times with 0.15 M NaCl for 10 min at 4°C, then incubated in 1% ammonium sulfide solution for 20 min at 4°C. Finally, the sections were washed three times with 0.15 M NaCl for 5 min at 4°C, then examined on a glass slide with a mounting medium comprising glycerin: PBS (9:1).

Immunofluorescence staining analysis of CD11c: To validate the above histochemistry staining results, immunofluorescence staining was performed using an antibody against CD11c, a dendritic cell marker. All steps were performed in the manner described above for immunofluorescence staining of connexin 43, except that the primary and secondary antibodies were mouse anti-CD11c/Integrin Alpha X (60258-1; Proteintech Group Inc., Rosemont, IL, USA) diluted 1:1,000 without Can Get Signal and CF 543-conjugated goat anti-mouse IgG serum (diluted 1:300; Biotium), respectively.

For additional validation, cells immediately below the corneal epithelium were subjected to double immunofluorescence staining with antibodies against CD11c and connexin 43. Tissue sections were subjected to immunofluorescence staining of CD11c as described above, then washed without cover glass. Subsequently, the sections were subjected to immunofluorescence staining of connexin 43 as described above.

Statistical analysis

The distributions of keratocytes were analyzed by comparing the numbers of cells in the central and limbal areas of the cornea. The Bonferroni method was used to compare the numbers of cells on the epithelial, central, and endothelial sides ($P<0.05$).

RESULTS

Observation of cells in corneal stroma

Light microscopy analysis of stromal cell distribution: The epithelial, middle, and endothelial sides of the central and limbal areas of the corneal stroma are shown in Fig. 1. There were 89 ± 15 corneal keratocytes in the central area and 98 ± 15 corneal keratocytes in the limbal area. Although these values did not significantly differ, the number of keratocytes in corneal stroma tissues tended to be higher in the limbus than in the central area (Fig. 2). The numbers of cells were compared among different zones (epithelium, middle, and endothelium side) in each area. In the central area, these values were 117 ± 19, 87 ± 19, and 71 ± 16 in the epithelium, middle, and endothelium sides, respectively; in the limbal area, they were 124 ± 18, 90 ± 15, and 80 ± 16, respectively. The numbers of keratocytes in the middle and endothelial sides of the central area were significantly lower (74% and 61%, respectively) than the number on the epithelial side; these numbers in the limbus area were also significantly decreased (73% and 65%, respectively) (Fig. 2).

Transmission electron microscopy analysis of ultrastructural morphology: The nuclear areas of the keratocytes are shown in Fig. 3. The keratocytes on the epithelial side had thin nuclear areas and elongated cells with long cytoplasmic processes (Fig. 3a, 3b). In contrast, keratocytes on the endothelial side were flat but had a thick nuclear area with an embedded nuclear membrane (Fig. 3c, 3d) and many organelles (e.g., lysosomes and phagosome), as shown in Fig. 3e, 3f. Additionally, there were cells with a large nuclear area and no spindle shape immediately below the epithelium (Fig. 4).

Scanning electron microscopy analysis of keratocyte meshwork: Keratocytes extended their cytoplasmic processes in many directions, forming a dense meshwork between keratocytes. In particular, keratocytes on the limbal epithelial side had a large number of cells and extended many thin cytoplasmic processes in multiple directions, leading to a dense meshwork between keratocytes. In contrast, the meshwork on the central endothelial side was sparse (Fig. 5).

Observation of gap junctions among keratocytes

Immunofluorescence staining analysis of connexin 43: Connexin 43 was expressed throughout the cytoplasm, and the cytoplasmic
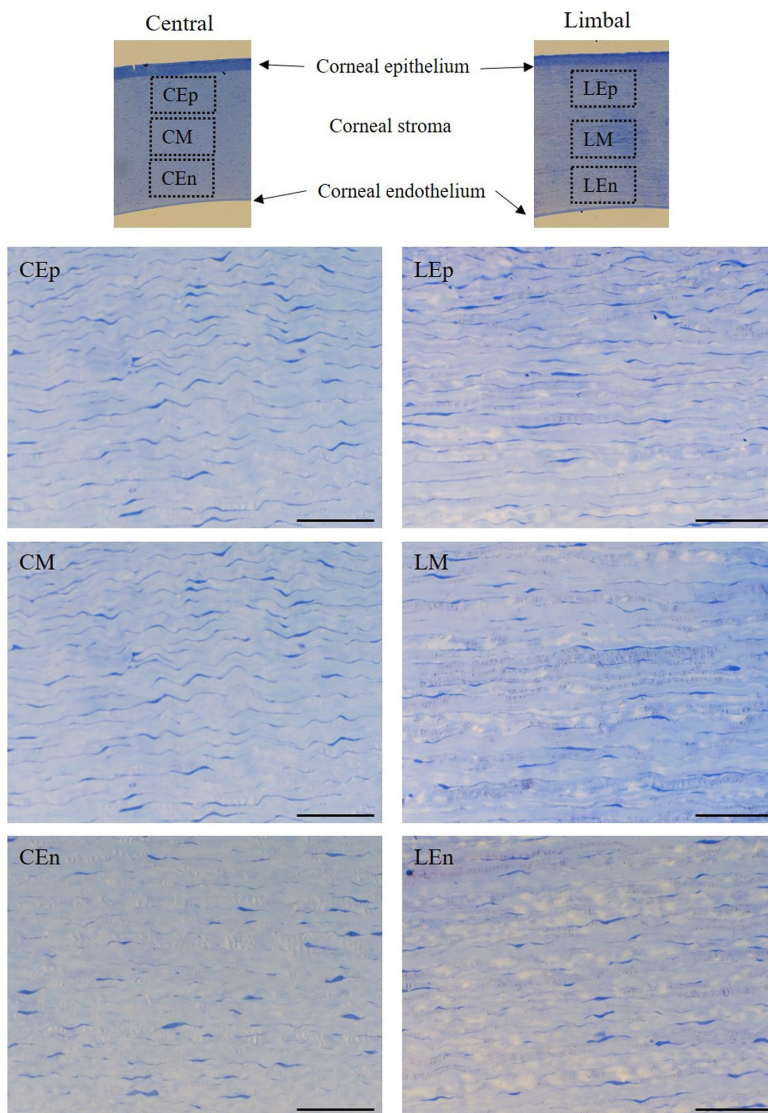
Fig. 1. Distribution of corneal keratocytes in the corneal stroma, as determined by toluidine blue staining. The two upper figures show the overall view of central and limbal areas. The lower six panels represent magnified images of each layer; left panels show the central area and right panels show the limbal area. Flat corneal keratocytes were stained blue and long cytoplasmic processes were observed between the light blue collagen layers in all areas. In all areas, blue-stained flat keratocytes and long, elongated cytoplasmic processes were observed between the light blue-stained collagen layers. CEp, central epithelial side; CM, central middle side; CEn, central endothelial side; LEp, limbal epithelial side; LM, limbal middle side; LEn, limbal endothelial side. Bars=50 μm.
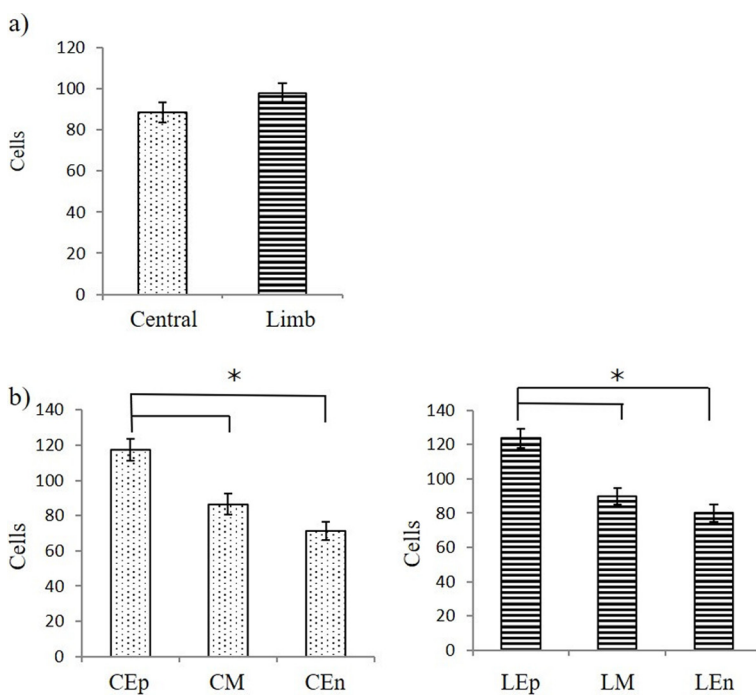

Fig. 2. Number of keratocytes in the corneal stroma. (**a**) Number of keratocytes per unit area in central and limbal areas of the corneal stroma. The number of keratocytes tended to be higher in the limbal area than in the central area. (**b**) Number of keratocytes per unit area in each area of the corneal stroma. The number of keratocytes per unit area tended to decrease from the epithelial to the endothelial side in both central and limbal areas. The number of cells was significantly higher on the epithelial side than on the endothelial side. $*P<0.05$. CEp, central epithelial side; CM, central middle side; CEn, central endothelial side; LEp, limbal epithelial side; LM, limbal middle side; LEn, limbal endothelial side.
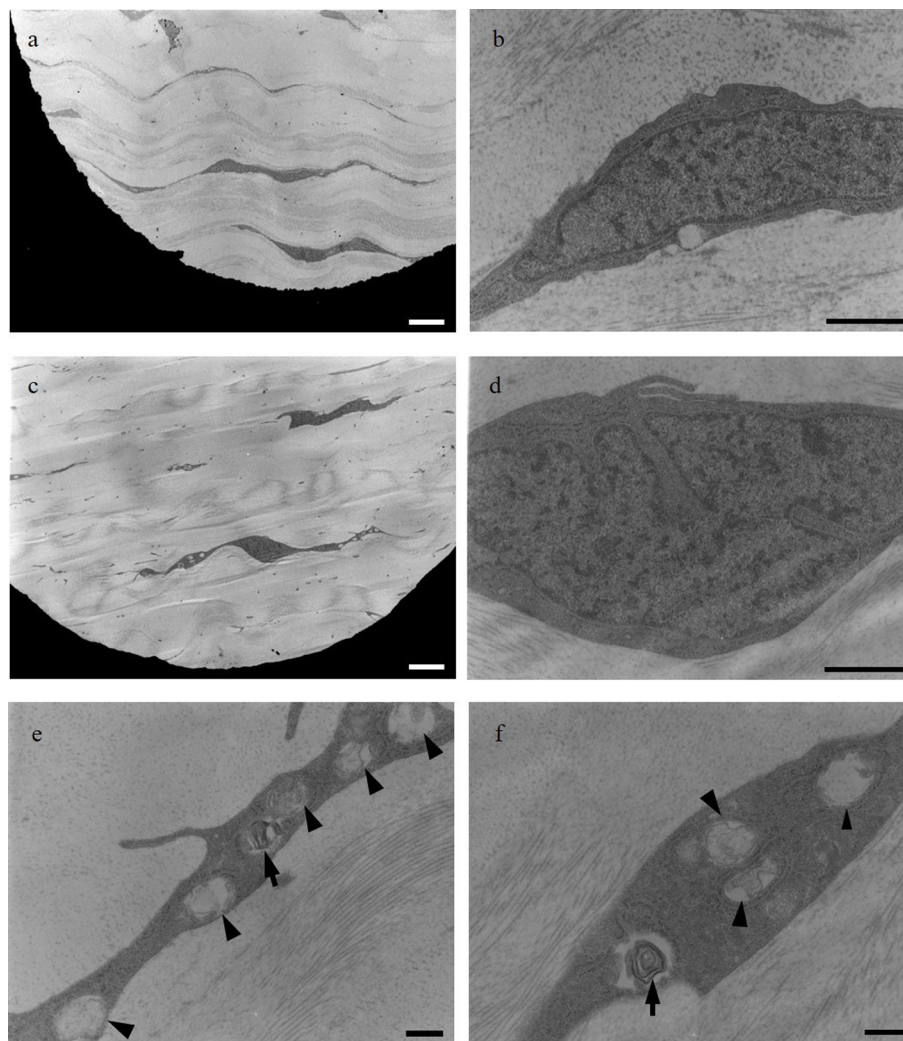
Fig. 3. Corneal keratocytes observed by transmission electron microscopy. Panels **a** and **b** depict the epithelial side at low and high magnification, respectively; panels **c** and **d** depict the endothelial side. Corneal keratocytes on the epithelial side exhibited a thin nuclear area and long cytoplasmic processes. Corneal keratocytes on the endothelial side exhibited a large nuclear area and nuclear membrane depression. Panels **e** and **f** depict intracellular organelles in keratocytes on the endothelial side. Corneal keratocytes exhibited many lamellar lysosomes (arrows) and phagosomes (arrowheads). Bars in a and c=5 µm. Bars in b and d=1 µm. Bars in e and f=500 nm.

processes were connected to each other (Fig. 6). The cytoplasmic processes extended horizontally along the collagen layer, but some cells exhibited vertical extensions that were connected to the cytoplasmic processes. Additionally, cytoplasmic processes without nuclei were observed in a wide area between collagen layers.

Transmission electron microscopy analysis of cell junctions: Neighboring cells were connected to each other by the cytoplasm contents of the extended cytoplasmic processes (where electron density was high) (Fig. 7a, 7b). In cell bodies with nuclei, adjacent cells were also connected to each other (Fig. 7c, 7d). Additionally, only cytoplasmic processes were observed in some areas. Under observation at low magnification, scattered cytoplasmic processes (easily identified by heavy metal block staining) were observed in the corneal stroma (Fig. 7e).

Observation of immunocytes in corneal stroma

Analysis of ATPase-positive immunocompetent cells: ATPase-positive immunocompetent cells were found only on the epithelial side; they were absent from the endothelial and middle side in both central and limbal areas of the cornea (Fig. 8).

Immunofluorescence staining analysis of CD11c: Cells expressing CD11c with high fluorescence intensity and arranged along a few layers were found immediately below the corneal epithelium in central and limbal areas (Fig. 9).

Additionally, cells co-expressing connexin 43 and CD11c at high fluorescence intensity were observed immediately below the corneal epithelium (Fig. 9). The all CD11c-positive cells also had extended connexin 43-positive cytoplasmic processes, similar to corneal keratocytes.
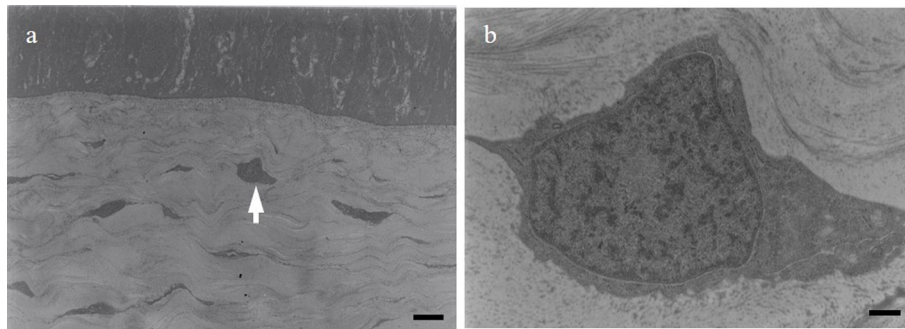
Fig. 4. A representative cell located immediately below the epithelial side. The cell indicated by an arrowhead in left panel **a** differs from the typical keratocyte shape observed in the limbal epithelium side; it exhibits a large and circular nuclear region. Panel **b** shows a magnified view of that cell. Bar in a=50 μm. Bar in b=500 nm.
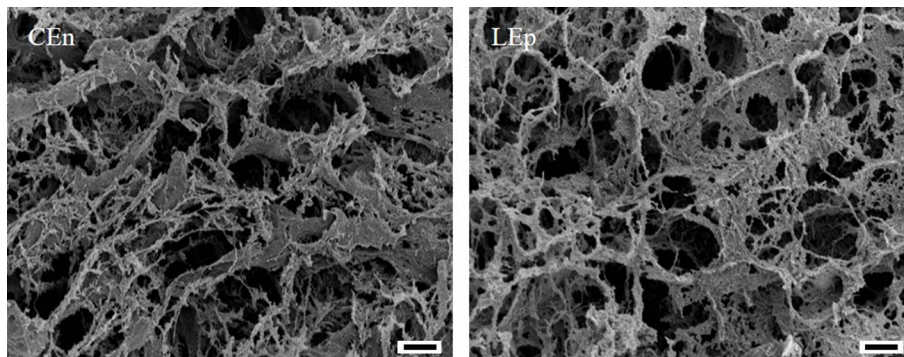

Fig. 5. Keratocyte meshwork structure observed by scanning electron microscopy. Panel CEn shows the endothelial side of the central cornea, while panel LEp shows the epithelial side of the limbus. The meshwork in panel LEp shows many thin cytoplasmic processes extending in multiple directions; it is denser than the meshwork in panel CEn. Bars=10 μm.
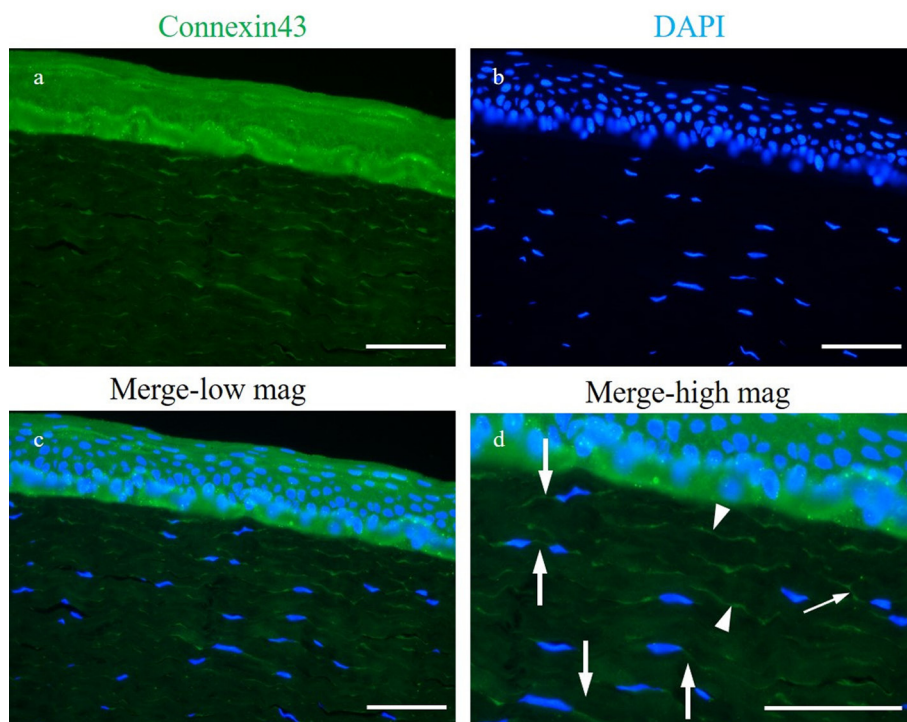

Fig. 6. Immunofluorescence analysis of keratocytes on the epithelial side in the central area, revealing the patterns of gap junction (connexin 43; panel **a**, green) protein expression and nuclear staining (DAPI; panel **b**, blue). Panel **c** depicts a merged image of panels a and b. Panel **d** shows a magnified image of panel c. Connexin 43 is expressed in corneal stroma, in areas where corneal cells are in contact with each other. Large arrows indicate gap junctions expressed around the nucleus along the cytoplasm. Arrowheads indicate gap junctions connecting processes of adjacent cells, although nuclei are not identified. Small arrow indicates cell processes vertically connected via gap junctions. Bars=50 μm.
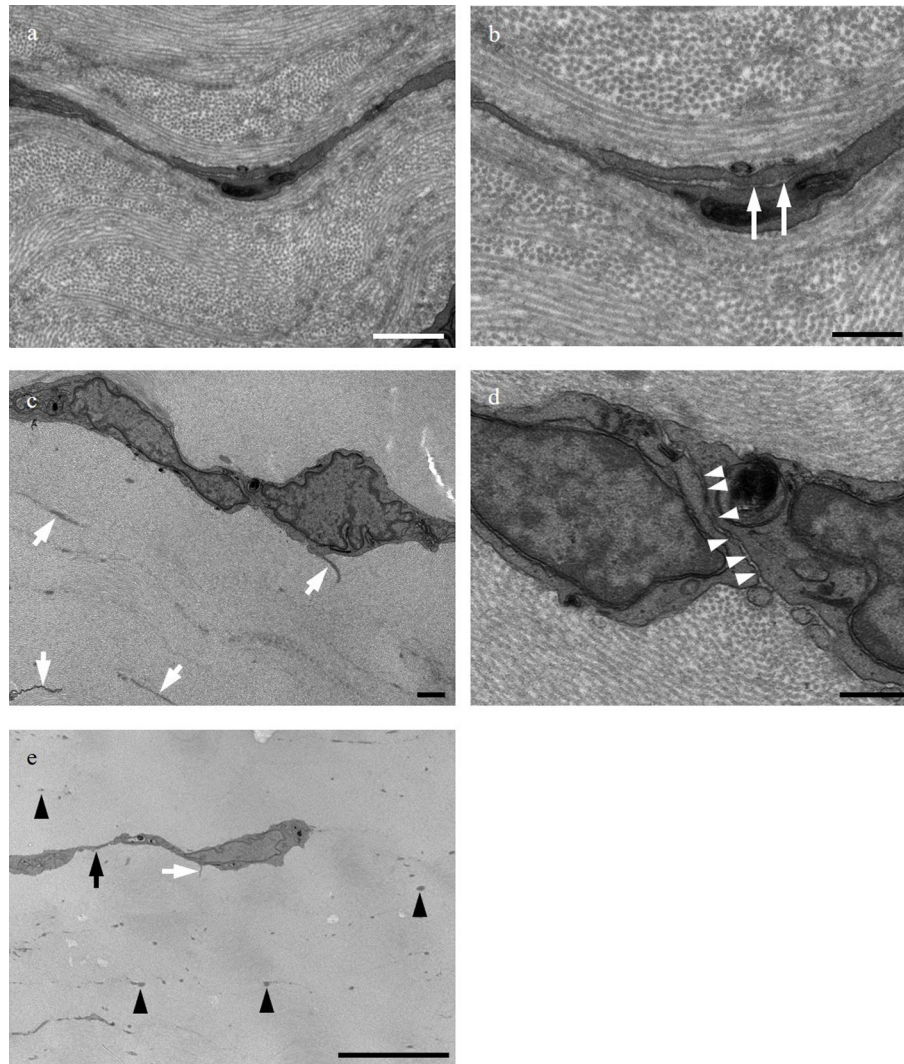
Fig. 7. Transmission electron microscopy image of the cellular junction. Panels **a** and **b** are low and high magnification images, respectively, of the epithelial side in the limbal area. Cytoplasmic processes are connected to each other at cell surfaces. Arrows indicate connections with high electron density. Panels **c** and **d** are low and high magnification images, respectively, of the epithelial side in the limbal area. Images depict cytoplasm connections between collagen layers where two cells with nuclei are connected at cell surfaces. Arrowheads indicate connections with high electron density. Arrows indicate abundant cytoplasmic processes around the cells. Panel **e** depict electron micrograph of corneal stroma observed at very low magnification. Many scattered cell processes were identified. White arrow indicates cytoplasmic process that connect to the cell body. Arrowheads indicate cytoplasmic projections with electron density identical to the cell body are scattered in the corneal stroma. Black arrow indicates a connection between cytoplasmic processes. The photo is representative of findings in the limbal epithelium area. Bars in a and c=1 μm. Bars in b and d=500 nm. Bar in e=10 μm.

DISCUSSION

In the present study, light microscopy showed that corneal cells were primarily located in the limbus, rather than the center of the cornea. This may reflect the distribution of cells during corneal development, as follows. During corneal development, keratocytes and corneal endothelium reportedly originate from neural crest-derived cells [3]. Some neural crest-derived cells migrate between the corneal epithelium and lens vacuole; subsequently, they migrate from the limbus to the center, forming the corneal endothelium. They also migrate from the limbus to the center between the epithelium and endothelium, becoming keratocytes [6] (Supplementary Data 1, 2). After development, keratocyte stem cells reportedly reside near the corneal limbus, along with corneal epithelial stem cells [4]. The area around the corneal limbus is thus presumed to constitute the point of corneal development and turnover; corneal cells migrate from the corneal limbus to the center of the cornea. Keratocyte turnover occurs over a period of several years in humans, while corneal epithelium turnover occurs over a period of 1–2 weeks [18]. Because the eyes used in this study were obtained from actively growing 6-month-old pigs, TUNEL analysis did not reveal cells with DNA fragmentation (Supplementary Data 1, 2). Thus, the pigs used in this experiment did not exhibit cellular turnover within the corneal stroma; this presumably reflects the cellular
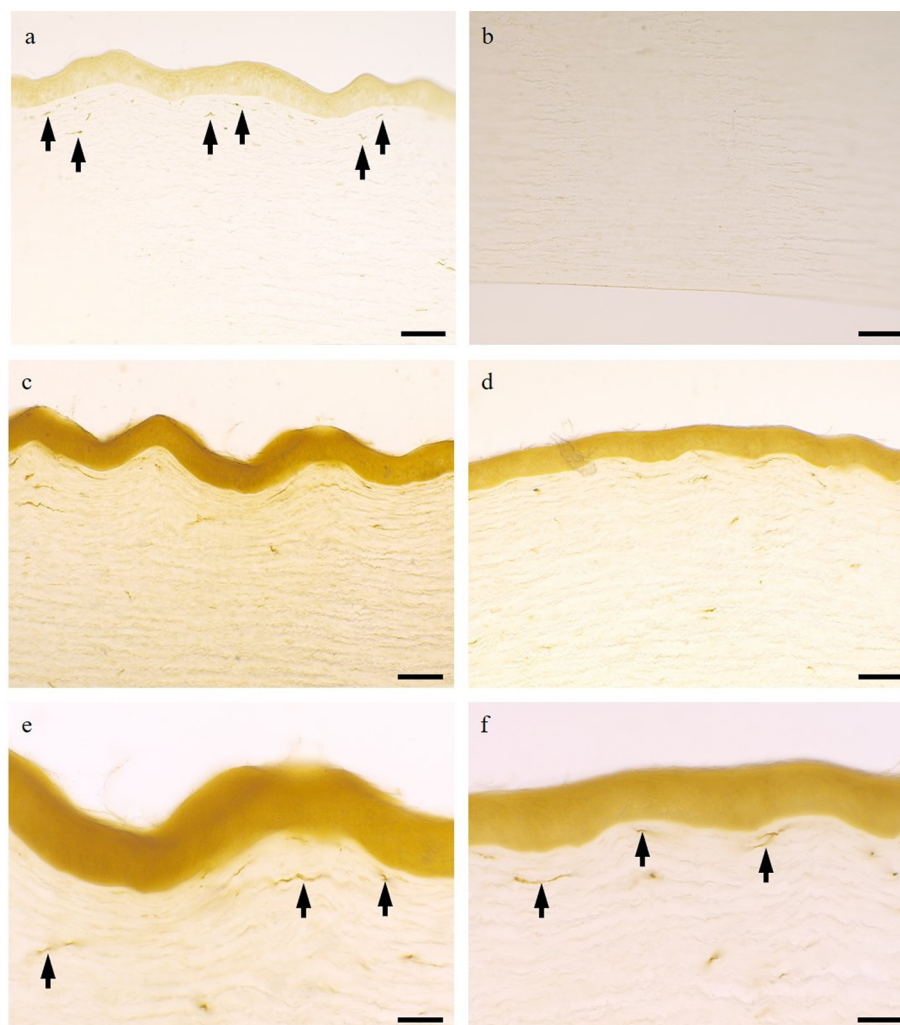
Fig. 8. Adenosine triphosphatase (ATPase) staining image of intrinsic corneal stroma. Panel **a** shows the epithelial side of the central cornea, while panel **b** shows the endothelial side of the central cornea. ATPase-positive immunocompetent cells (arrows) were mainly observed on the epithelial side, not on the endothelial side. Panels **c** and **e** depict the epithelial side of the central cornea at low and high magnification, respectively; panels **d** and **f** depict the epithelial side of the limbus at low and high magnification, respectively. ATPase-positive immunocompetent cells (arrows) mainly were located immediately below the epithelium in central and limbal areas. Bars in a, b, c and d=100 μm. Bars in e and f=50 μm.

distribution during corneal development. The corneal limbus reportedly contains capillaries that provide cells with fluid factors such as blood-derived cytokines that are necessary for cell differentiation; this creates a microenvironment necessary for differentiation [5]. Furthermore, keratocyte progenitor cells isolated from the corneal limbus exhibit higher proliferative activity in cell culture than do progenitor cells isolated from the central cornea [23]. Considering these previous findings, we hypothesized that greater numbers of keratocytes tend to be located in the limbus than in the cornea because cell differentiation and proliferation are more active in the limbus than in the central area.

Transmission electron microscopy revealed that the long diameter of keratocyte was largest on the epithelial side of the corneal limbus, while the short diameter was largest on the endothelial side of the central cornea. These region-specific differences in cellular shape may arise from the following factors. Cell growth factors, cytokines, and interactions with corneal epithelial cells reportedly affect the maintenance of keratocyte morphology and morphological changes [13–17]. In the normal and resting state, keratocytes are flattened cells. The cytoplasm contains small amounts of intracellular organelles such as the Golgi complex, rough endoplasmic reticulum, and mitochondria; keratocytes thus are quiet cells with low metabolic activity [2]. Keratocytes extend elongated cell processes in multiple directions and connect with neighboring cells via gap junctions, forming a meshwork within the corneal stromal matrix [24]. However, activated keratocytes become larger and develop organelles [39]. In particular, when a wound extends into the corneal matrix, corneal stromal cells at the wound site undergo apoptosis. Surrounding keratocytes are activated and transformed by the removal of gap junctions via processes; they participate in wound healing by migrating to the wound site, phagocytosing wounded tissue, and synthesizing collagen [20]. Additionally, cells with high transcriptional activity have been reported to exhibit nuclear membrane entrapment because of the binding of nuclear lamina and chromosomes [21]. These results suggest that keratocytes with large short diameters, large nuclear areas, and depressed nuclear membranes found in the central endothelial side are cells with
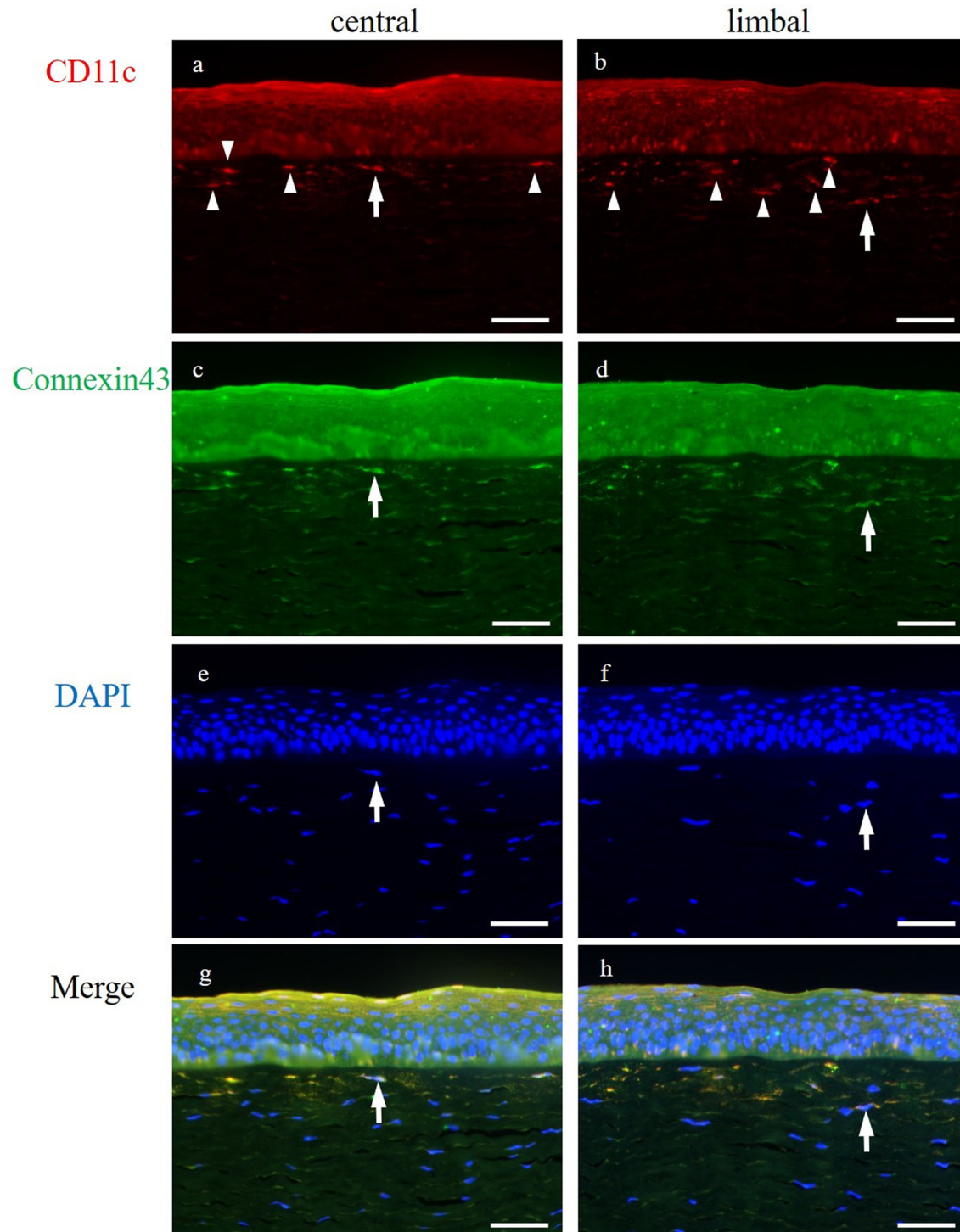
Fig. 9. Immunofluorescence analysis of keratocytes on the epithelial side, revealing the patterns of CD11c (panels **a** and **b**, red), gap junction (connexin 43; panels **c** and **d**, green) protein expression and nuclear staining (DAPI; panels **e** and **f**, blue). Panel **g** is a merged image of panels a, c and e. Panel **h** is a merged image of panels b, d and f. CD11c expression was arranged in a few layers immediately below the epithelium (arrowheads). The merged images show CD11c expression around the nucleus (arrows). In addition, the merged images revealed cells co-expressing CD11c and connexin 43 (arrows) immediately below the corneal epithelium in both central and limbal areas of the cornea. These cells also extended processes into the cytoplasm and were associated with neighboring cells. The photos are representative of findings in the central and limbal epithelium area. Bars=50 μm.

high transcriptional activity. Thus, cells distributed on the endothelial side are presumably the main components of collagen renewal; moreover, keratocytes differ in morphology and function according to region and distribution.

Comparison of the numbers of corneal cells between epithelial and endothelial sides showed that there were significantly more

corneal cells on the epithelial side in both the central and limbus areas (Fig. 2b). This evidence from scanning electron microscopy indicated that the meshwork structure of corneal cells was more dense on the epithelial side than on the endothelial side. Research involving three-dimensional cultures of corneal cells using collagen gels has demonstrated that the morphology of keratocytes, which are connected by gap junctions between cell processes, flattens with increasing cell density [19]. These three-dimensional culture findings supported the present *in vivo* results in terms of regional differences in the distribution and ultrastructural morphology of keratocytes between the epithelial and endothelial sides of the corneal stroma.

In vivo electron microscopy observations of corneal stroma have demonstrated that keratocyte processes are connected by gap junctions [37]. In the present study, gap junctions between cells in the corneal stroma were found on the surfaces of cytoplasmic processes (Fig. 7a, 7b). Furthermore, cytoplasm connections were observed (Fig. 7c, 7d), which suggested that some of the keratocytes observed by light microscopy comprised aggregates of multiple cells. In addition to the conventional transmission electron microscopy findings, we performed transmission electron microscopy observation using osmium-thiocarbohydrazide-osmium staining, which emphasizes the outline of the cytoplasm; the results revealed many cytoplasmic processes scattered three-dimensionally in the corneal stroma. Furthermore, immunofluorescence staining of connexin 43 showed that the cytoplasmic processes were connected both vertically and horizontally. These results suggest that the horizontally spreading network via gap junctions of keratocytes with distinct densities among layers is also vertically connected, thus conveying three-dimensional information to all corneal stroma. Consequently, changes in the environment within one keratocyte are rapidly transmitted to neighboring keratocytes, which function as intercellular network [38]. This rapid cell communication via gap junctions between collagen-producing cells in connective tissue is also observed in tendon cells [8]; it is presumed to maintain a high level of function in fibrous connective tissue. In corneal stroma, defense mechanisms are carried out by the keratocyte meshwork; intercellular signaling occurs via gap junctions [38]. Therefore, the high number of keratocytes on the epithelial side and the formation of a dense meshwork structure may be necessary to support the rapid response to external stimuli, trauma, and inflammation at the ocular surface (e.g., upon exposure to toxic substances); they may also be necessary to ensure wound healing [38].

ATPase-positive and CD11c-positive cells, which differ in shape and size from the keratocytes located immediately below the epithelium, are presumed to be antigen-presenting cells [10, 32]. The corneal epithelium, which contacts the external environment through the tear layer, must prevent the invasion of foreign matter while maintaining corneal transparency. Therefore, the cornea's fluid-based defense mechanisms include mucin, lactoferrin, lysozyme, and secretory IgA, all of which are present in tear fluid. In terms of physical and biological defense mechanisms, the corneal epithelium contains Langerhans cells, adhesion molecules, and immunocompetent cells [31]. Recent studies have shown that antigen-presenting cells are also present in the corneal stroma, and they are suspected to participate in corneal rejection [7, 28]. In the present study, ATPase-positive and CD11c-positive cells were found in the corneal stroma immediately below the epithelium. Consequently, cells with large nuclear area and no spindle shape, observed immediately below the epithelium via electron microscopy (Fig. 4), were presumed to be antigen-presenting cells. This finding indicates that antigen-presenting cells, which have been previously reported only in humans and rodents, are also present in the subepithelial stroma of pigs. Additionally, CD11c-positive cells were also connexin 43-positive. This finding suggests that these co-expressing cells extend their cytoplasmic processes to connect with adjacent keratocytes. Furthermore, this finding implies that CD11c-positive immune cells participate in an extensive network of corneal cells.

This study revealed that, in 6-month-old pigs, keratocytes exhibit the features shown in Fig. 10. In the corneal stroma, corneal keratocytes are abundantly distributed on the epithelial side. Additionally, healthy keratocytes maintain a flattened morphology with extended cell processes because of interactions with cytokines and epithelium. Because of the large number of cells distributed on the epithelial side of the corneal stroma and the large number of long, extended cell processes, a dense meshwork is constructed via
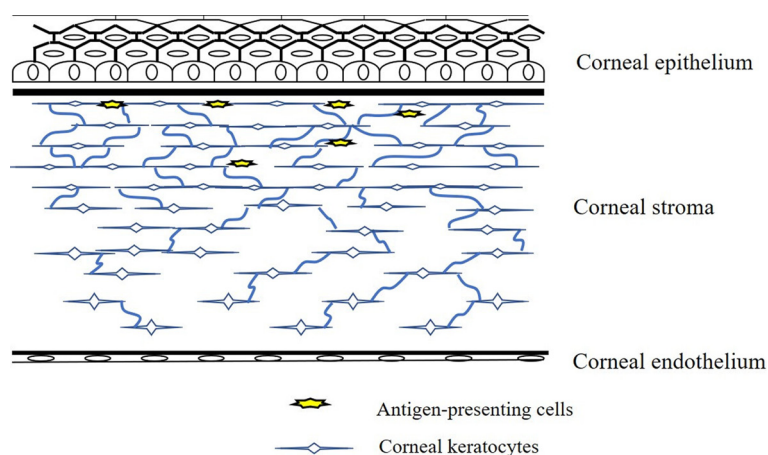

Fig. 10. Schematic diagram showing the distributions of keratocytes and immunocompetent cells in the cornea. Keratocytes with large short diameters are distributed on the endothelial side of the cornea; these cells are highly transcriptionally active and are presumed to function mainly in collagen renewal. In contrast many stationary keratocytes with large diameters are distributed on the epithelial side of the cornea; they form a dense meshwork with immunocompetent cells.

gap junctions between cells. Furthermore, gap junctions extend in the vertical direction and form an extensive network of keratocytes throughout the corneal stroma. If the corneal epithelium barrier is broken, keratocytes presumably react quickly to reduce harm to deeper layers; antigen-presenting cells located immediately below the corneal epithelium also participate in the meshwork, thus strengthening the defense mechanism. In summary, keratocytes and immune cells distributed immediately below the corneal epithelial are closely related; furthermore, the gap junction-mediated communication of keratocytes from the epithelial to the endothelial side forms a large functional intercellular network throughout the corneal stroma. Thus, keratocytes distributed on the epithelial side maintain a morphology that participates in biological defenses (e.g., wound healing and immunity), which suggests that they participate in corneal homeostasis.

CONFLICT OF INTEREST. The authors declare no conflict of interest.

REFERENCES

1. Borcherding MS, Blacik LJ, Sittig RA, Bizzell JW, Breen M, Weinstein HG. 1975. Proteoglycans and collagen fibre organization in human corneoscleral tissue. *Exp Eye Res* **21**: 59–70. [Medline] [CrossRef]
2. Bron AJ, Tripathi RC, Tripathi BJ. 1997. The cornea and sclera. pp. 233–278. In: Wolff's Anatomy of the Eye and Orbit, Chapman & Hall Medicine, London.
3. Creuzet S, Vincent C, Couly G. 2005. Neural crest derivatives in ocular and periocular structures. *Int J Dev Biol* **49**: 161–171. [Medline] [CrossRef]
4. Du Y, Funderburgh ML, Mann MM, SundarRaj N, Funderburgh JL. 2005. Multipotent stem cells in human corneal stroma. *Stem Cells* **23**: 1266–1275. [Medline] [CrossRef]
5. Ebrahimi M, Taghi-Abadi E, Baharvand H. 2009. Limbal stem cells in review. *J Ophthalmic Vis Res* **4**: 40–58. [Medline]
6. Feneck EM, Lewis PN, Meek KM. 2020. Identification of a primary stroma and novel endothelial cell projections in the developing human cornea. *Invest Ophthalmol Vis Sci* **61**: 5. [Medline] [CrossRef]
7. George AJT, Larkin DFP. 2004. Corneal transplantation: the forgotten graft. *Am J Transplant* **4**: 678–685. [Medline] [CrossRef]
8. Hadate S, Takahashi N, Kametani K, Iwasaki T, Hasega Y, Tangkawattana P, Kawasaki T, Ueda H, Hosotani M, Watanabe T. 2020. Ultrastructural study of the three-dimensional tenocyte network in newly hatched chick Achilles tendons using serial block face-scanning electron microscopy. *J Vet Med Sci* **82**: 948–954. [Medline] [CrossRef]
9. Hahn RA, Birk DE. 1992. beta-D xyloside alters dermatan sulfate proteoglycan synthesis and the organization of the developing avian corneal stroma. *Development* **115**: 383–393. [Medline] [CrossRef]
10. Hamrah P, Huq SO, Liu Y, Zhang Q, Dana MR. 2003. Corneal immunity is mediated by heterogeneous population of antigen-presenting cells. *J Leukoc Biol* **74**: 172–178. [Medline] [CrossRef]
11. Hattori T, Chauhan SK, Lee H, Ueno H, Dana R, Kaplan DH, Saban DR. 2011. Characterization of Langerin-expressing dendritic cell subsets in the normal cornea. *Invest Ophthalmol Vis Sci* **52**: 4598–4604. [Medline] [CrossRef]
12. Hayashi R, Ishikawa Y, Sasamoto Y, Katori R, Nomura N, Ichikawa T, Araki S, Soma T, Kawasaki S, Sekiguchi K, Quantock AJ, Tsujikawa M, Nishida K. 2016. Co-ordinated ocular development from human iPS cells and recovery of corneal function. *Nature* **531**: 376–380. [Medline] [CrossRef]
13. Hibino T, Wada Y, Mishima H, Otori T. 1998. The effect of corneal epithelial cells on the collagen gel contraction by keratocytes. *Jpn J Ophthalmol* **42**: 174–179. [Medline] [CrossRef]
14. Jester JV, Barry PA, Lind GJ, Petroll WM, Garana R, Cavanagh HD. 1994. Corneal keratocytes: in situ and in vitro organization of cytoskeletal contractile proteins. *Invest Ophthalmol Vis Sci* **35**: 730–743. [Medline]
15. Ko JA, Liu Y, Yanai R, Chikama T, Takezawa T, Nishida T. 2008. Upregulation of tight-junctional proteins in corneal epithelial cells by corneal fibroblasts in collagen vitrigel cultures. *Invest Ophthalmol Vis Sci* **49**: 113–119. [Medline] [CrossRef]
16. Ko JA, Morishige N, Yanai R, Nishida T. 2008. Up-regulation of semaphorin 3A in human corneal fibroblasts by epidermal growth factor released from cocultured human corneal epithelial cells. *Biochem Biophys Res Commun* **377**: 104–108. [Medline] [CrossRef]
17. Ko JA, Yanai R, Morishige N, Takezawa T, Nishida T. 2009. Upregulation of connexin43 expression in corneal fibroblasts by corneal epithelial cells. *Invest Ophthalmol Vis Sci* **50**: 2054–2060. [Medline] [CrossRef]
18. Lagali N. 2020. Corneal stromal regeneration: current status and future therapeutic potential. *Curr Eye Res* **45**: 278–290. [Medline] [CrossRef]
19. Lakshman N, Kim A, Petroll WM. 2010. Characterization of corneal keratocyte morphology and mechanical activity within 3-D collagen matrices. *Exp Eye Res* **90**: 350–359. [Medline] [CrossRef]
20. Lande MA, Birk DE, Nagpal ML, Rader RL. 1981. Phagocytic properties of human keratocyte cultures. *Invest Ophthalmol Vis Sci* **20**: 481–489. [Medline]
21. Ma Y, Cai S, Lv Q, Jiang Q, Zhang Q, Sodmergen, Zhai Z, Zhang C. 2007. Lamin B receptor plays a role in stimulating nuclear envelope production and targeting membrane vesicles to chromatin during nuclear envelope assembly through direct interaction with importin beta. *J Cell Sci* **120**: 520–530. [Medline] [CrossRef]
22. Marshall GE, Konstas AG, Lee WR. 1993. Collagens in ocular tissues. *Br J Ophthalmol* **77**: 515–524. [Medline] [CrossRef]
23. Mimura T, Amano S, Yokoo S, Uchida S, Usui T, Yamagami S. 2008. Isolation and distribution of rabbit keratocyte precursors. *Mol Vis* **14**: 197–203. [Medline]
24. Nagayasu A, Hirayanagi T, Tanaka Y, Tangkawattana P, Ueda H, Takehana K. 2009. Site-dependent differences in collagen lamellae in the corneal substantia propria of beagle dogs. *J Vet Med Sci* **71**: 1229–1231. [Medline] [CrossRef]
25. Nagayasu A, Yokoi H, Minaguchi JA, Hosaka YZ, Ueda H, Takehana K. 2012. Efficacy of self-assembled hydrogels composed of positively or negatively charged peptides as scaffolds for cell culture. *J Biomater Appl* **26**: 651–665. [Medline] [CrossRef]
26. Nakamura T, Ishikawa F, Sonoda KH, Hisatomi T, Qiao H, Yamada J, Fukata M, Ishibashi T, Harada M, Kinoshita S. 2005. Characterization and distribution of bone marrow-derived cells in mouse cornea. *Invest Ophthalmol Vis Sci* **46**: 497–503. [Medline] [CrossRef]
27. Nishida K, Yamato M, Hayashida Y, Watanabe K, Yamamoto K, Adachi E, Nagai S, Kikuchi A, Maeda N, Watanabe H, Okano T, Tano Y. 2004. Corneal reconstruction with tissue-engineered cell sheets composed of autologous oral mucosal epithelium. *N Engl J Med* **351**: 1187–1196. [Medline] [CrossRef]
28. Nishida T, Yasumoto K, Otori T, Desaki J. 1988. The network structure of corneal fibroblasts in the rat as revealed by scanning electron microscopy. *Invest Ophthalmol Vis Sci* **29**: 1887–1890. [Medline]

29. Okubo T, Hayashi R, Shibata S, Kudo Y, Ishikawa Y, Inoue S, Kobayashi Y, Honda A, Honma Y, Kawasaki S, Nishida K. 2020. Generation and validation of a PITX2-EGFP reporter line of human induced pluripotent stem cells enables isolation of periocular mesenchymal cells. *J Biol Chem* **295**: 3456–3465. [Medline] [CrossRef]

30. Rada JA, Cornuet PK, Hassell JR. 1993. Regulation of corneal collagen fibrillogenesis in vitro by corneal proteoglycan (lumican and decorin) core proteins. *Exp Eye Res* **56**: 635–648. [Medline] [CrossRef]

31. Resch MD, Imre L, Tapaszto B, Nemeth J. 2008. Confocal microscopic evidence of increased Langerhans cell activity after corneal metal foreign body removal. *Eur J Ophthalmol* **18**: 703–707. [Medline] [CrossRef]

32. Sankaridurg PR, Rao GN, Rao HN, Sweeney DF, Holden BA. 2000. ATPase-positive dendritic cells in the limbal and corneal epithelium of guinea pigs after extended wear of hydrogel lenses. *Cornea* **19**: 374–377. [Medline] [CrossRef]

33. Scott JE. 1988. Proteoglycan-fibrillar collagen interactions. *Biochem J* **252**: 313–323. [Medline] [CrossRef]

34. Stark WJ. 1980. Transplantation immunology of penetrating keratoplasty. *Trans Am Ophthalmol Soc* **78**: 1079–1117. [Medline]

35. Sumide T, Nishida K, Yamato M, Ide T, Hayashida Y, Watanabe K, Yang J, Kohno C, Kikuchi A, Maeda N, Watanabe H, Okano T, Tano Y. 2006. Functional human corneal endothelial cell sheets harvested from temperature-responsive culture surfaces. *FASEB J* **20**: 392–394. [Medline] [CrossRef]

36. Traboulsi EI. 1998. Ocular malformations and developmental genes. *J AAPOS* **2**: 317–323. [Medline] [CrossRef]

37. Ueda A, Nishida T, Otori T, Fujita H. 1987. Electron-microscopic studies on the presence of gap junctions between corneal fibroblasts in rabbits. *Cell Tissue Res* **249**: 473–475. [Medline] [CrossRef]

38. Watsky MA. 1995. Keratocyte gap junctional communication in normal and wounded rabbit corneas and human corneas. *Invest Ophthalmol Vis Sci* **36**: 2568–2576. [Medline]

39. West-Mays JA, Dwivedi DJ. 2006. The keratocyte: corneal stromal cell with variable repair phenotypes. *Int J Biochem Cell Biol* **38**: 1625–1631. [Medline] [CrossRef]

40. Yamagami S, Ebihara N, Usui T, Yokoo S, Amano S. 2006. Bone marrow-derived cells in normal human corneal stroma. *Arch Ophthalmol* **124**: 62–69. [Medline] [CrossRef]